STUDY ON VERTICAL-AXIS WIND TURBINES USING STREAMTUBE AND DYNAMIC STALL MODELS

BY

DAVID VALLVERDÚ

Submitted in partial fulfillment of the
requirements for the degree of
TFG Exchange Program in Grau en Enginyeria en Tecnologies Aeroespacials
in the Graduate College of the
Illinois Institute of Technology
in collaboration with
Universitat Politècnica de Catalunya

Approved _____
Advisor

Chicago, Illinois
June 2014

ACKNOWLEDGEMENT

The production of this report wouldn't have been possible without the guidance and trust that my professor advisor, Dr. Dietmar Rempfer, deposited on me. Also, the invaluable dedication and help of my fellow office college and Master Graduate, Peter Kozak, has been decisive to my success and critical to overcome all obstacles and issues encountered. Thanks a lot to the rest of my office colleagues, who helped me and made my time working in IIT much more entertaining. Finally, I dedicate this report to all my old friends and family at home, specially my parents and sister for their support, and all the new friends I have made in this exciting stay in Chicago.

TABLE OF CONTENTS

ABSTRACT

The expected exhaustion of fossil sources of energy requires the improvement of other renewable sources, such as wind turbines. Vertical-axis wind turbines present very attractive performance characteristics but extremely complicated aerodynamics. Therefore, research is still needed on this field. A code is developed in order to apply the blade element momentum theory to these wind turbines. BEMT is shown to give considerably reliable results, compared to its fast convergence. BEMT is improved with dynamic stall and wake interaction modifications, in order to include more physical effects. Modified BEMT models will help obtain fast and qualitatively reliable data on VAWT performance. Comparisons with other authors prove that the generated code provides data that are close to the real results.

CHAPTER 2

STREAMTUBE MODEL

2.1 Concepts

This chapter develops and explains the streamtube model applied to performance prediction of vertical-axis wind turbines. Streamtube models are based on blade element method, a.k.a. BEM, and momentum theory. The combination is called blade element momentum theory, a.k.a. BEMT. Streamtube model is a relatively simple method, compared to finite volume or vortex modeling. The main advantage of this method is its ability to solve the domain without an internal volume mesh. However, to achieve this, the governing equations must be in integral form. Therefore, specially in a CFD case, they undergo very important simplifications.

The result is a very fast computational method with significant error in the final result – the amount of error is very dependent on the nature of the problem studied and, therefore, the governing equations. BEMT applications for VAWT cases give a fair approximation of the VAWT power output, especially for lower tip-speed ratios.

As said, BEMT applied to VAWTs is referred to as a streamtube model. As the name suggests, all streamtube models consist of applying each governing equation in its integral form to every one and each of the domains defined by the streamtubes. Each streamtube connects both inlet and outlet boundaries and is parallel to the velocity of the flow at all points. Therefore, there is no mass, momentum nor energy – neglecting thermal effects – exchange between adjacent streamtubes. This means that all components of the velocity perpendicular to the streamtubes are neglected. Hence, the turbine is being treated as a unidirectional flow problem only. This also

means that the streamtube section expansion due to flow energy loss and continuity is neglected[2].

Applying governing equations in their integral form entails the need of empirical data as an input to solve a turbine. Specifically, streamtube methods need the characteristic curves for lift and drag at any given angle of attack. Also, this method is unable to take into account turbulent effects such as wake interaction, very important at high TSR, or the influence of dynamic stall, dominant when the VAWT is working at low TSR and related to the empirical dependency. The following chapters discuss these issues.

2.2 Theory development

There are several versions of the streamtube model, each of them using a different boundary discretization. These variations are the single, multiple and double-multiple streamtube models, a.k.a. SST, MST and DMST, respectively.

STT, devised by Templin [28], considers the whole turbine as an actuator disk placed inside a single streamtube. MST, introduced by Strickland [24], improves SST by dividing the former single streamtube into multiple discrete streamtubes. Theoretical developments for both models can be found in Appendix A.

Finally DMST, proposed by Paraschivoiu [15] [16], improves MST by considering the turbine as two separate actuator disks – one for the upwind or front half-cycle and a second one for the downwind or rear half-cycle.

All streamtube models (BEMT) follow the same principle. First, they use the governing conservation equations to calculate the thrust force on each streamtube

[2]Paraschivoiu [18] proved that neglecting the streamtube section expansion, which induces spanwise velocity, does not introduce significant error – relatively to other omitted effects in BEMT application to VAWTs.

– the force parallel to it. Then, the same force is calculated from a load analysis. Both expressions depend on the flow velocity. Hence, they can be coupled to obtain a system of equations to solve the flow velocity field in the streamtube: the load analysis result is introduced into the momentum loss result. From the velocity field, all performance dependent variables of the turbine can be computed.

2.2.1 Governing equations

First of all, the three governing equations applied to any streamtube must be defined in integral formulation. These are mass, momentum and energy conservation[3], respectively

$$\frac{\mathrm{d}}{\mathrm{d}t}\int_{\Omega} \rho \,\mathrm{d}V + \oint_{\partial\Omega} \rho\, \boldsymbol{u}\cdot\boldsymbol{n}\,\mathrm{d}S = 0 \ , \tag{2.1}$$

$$\frac{\mathrm{d}}{\mathrm{d}t}\int_{\Omega} \rho\, \boldsymbol{u}\,\mathrm{d}V + \oint_{\partial\Omega} \rho\, \boldsymbol{u}\,(\boldsymbol{u}\cdot\boldsymbol{n})\,\mathrm{d}S = \sum \boldsymbol{F_{ext}} \tag{2.2}$$

and

$$\frac{\mathrm{d}}{\mathrm{d}t}\int_{\Omega} \rho\, u^2\,\mathrm{d}V + \oint_{\partial\Omega} \frac{1}{2}\rho\, u^2\,(\boldsymbol{u}\cdot\boldsymbol{n})\,\mathrm{d}S = -P \ , \tag{2.3}$$

where Ω is the domain where these equations are applied and $\boldsymbol{n}$ is a unit vector normal to $\partial\Omega$ and pointing outwards. $\sum \boldsymbol{F_{ext}}$ is the sum of the forces that the flow receives and P is the power output of the portion of the turbine inside the domain. Hence, $P > 0$ when the turbine is extracting energy from the flow. Bold symbols are vectors. Otherwise, they are scalars. BEMT treats the problem as a steady case, so all time derivate components from momentum and energy equations can be eliminated.

---

[3]Note that dynamic and other magnitudes that include dimension units – surface, volume, force, torque, power – have one less dimension than usual, because all the development is using 2D approach. For example, for a hypothetical force, F, the units are $[F] = N/m$

2.2.2 Physical definitions

One needs to define the geometry of a VAWT blade parametrically. Figure 2.1 is used for this purpose.

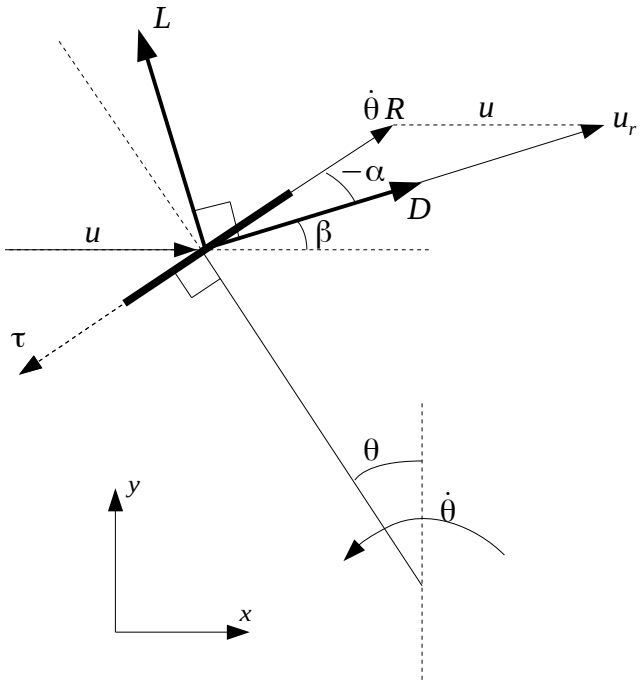

Figure 2.1: **Scheme of the flow velocities and forces from the blade point of view.** $\boldsymbol{\tau}$ is a unit vector tangent to the blade.

From it, the relative velocity (u_r) of the wind from the blade reference point of view,

$$\frac{u_r}{U_\infty} = \sqrt{\left(\frac{u}{U_\infty}\right)^2 + TSR^2 + 2\,\frac{u}{U_\infty}\,TSR\,\cos\theta}\ , \tag{2.4}$$

can be computed. Also, the flight path angle,

$$\beta = \arctan\left(\frac{TSR\,sin\theta}{u/U_\infty + TSR\,\cos\theta}\right)\ , \tag{2.5}$$

and the angle of attack,

$$\alpha = \text{modulus}\left(\frac{\pi + \beta - \theta}{2\pi}\right) - \pi \ , \tag{2.6}$$

will be needed.

Once the angle of attack is known, the lift, C_L, and drag, C_D, static coefficients of the VAWT blade profile can be obtained from experimental data[4],

$$L = \frac{1}{2}\,\rho\, c\, u_r^2\, C_L \tag{2.7}$$

and

$$D = \frac{1}{2}\,\rho\, c\, u_r^2\, C_D \ . \tag{2.8}$$

Note that the units of these forces are $[N/m]$: as said previously in this chapter, the turbine is approached as a 2D problem. Hence, all dynamic magnitudes lack one order of distance unit.

The whole force that the blade receives from the wind expressed as a function of lift and drag components,

$$\boldsymbol{F} = [D\,\cos\beta - L\,\sin\beta]\,\boldsymbol{i} + [D\,\sin\beta + L\,\cos\beta]\,\boldsymbol{j} \ , \tag{2.9}$$

is used to calculate the torque that the turbine receives from each blade,

$$\boldsymbol{T} = R\,\boldsymbol{F}\cdot\boldsymbol{t} = R\,(L\,\boldsymbol{l} + D\,\boldsymbol{d})\cdot\boldsymbol{\tau} \ , \tag{2.10}$$

where $\boldsymbol{l} = -\sin\beta\,\boldsymbol{i} + \cos\beta\,\boldsymbol{j}$, $\boldsymbol{d} = \cos\beta\,\boldsymbol{i} + \sin\beta\,\boldsymbol{j}$ and $\boldsymbol{\tau} = -\cos\theta\,\boldsymbol{i} - \sin\theta\,\boldsymbol{j}$. Therefore, the power coefficient obtained from one blade,

$$P = \frac{1}{2\pi}\int_0^{2\pi} \dot{\theta}\,T\,\mathrm{d}\theta \ , \tag{2.11}$$

is the result of averaging the instantaneous torque times the angular velocity along a period of azimuthal angle.

---

[4] Appendix B develops how these data sere obtained.

2.2.3 Double-multiple streamtube model

The most precise streamtube model is DMST, because it allows to consider the energy losses of the flow separately for the front and rear half of the VAWT. The flow is considered to travel through two consecutive actuator disks which, in turn, extract energy from it. Moreover, at the same time, the turbine domain is discretized in multiple streamtubes parallel to the flow, so a different velocity of the flow can be calculated at any position of the blade. Then, the contribution of all front and rear half-cycle streamtubes is added together. Figure 2.2 illustrates the DMST scheme. Observing Figure 2.2, one can distinguish five different states of the flow:

1. State $\boldsymbol{\infty}$: this is the free stream state. The flow is not perturbed by the turbine. It acts as the input state for Disk 1.

2. State **1**: this is the state of the flow when interacting with the upwind actuator disk, also called the front half-cycle of the turbine.

3. State $\boldsymbol{e}$: this is the equilibrium state. In this state, the flow is considered to be far enough from both disks, hence it is steady. This is an approximation. In reality, state $\boldsymbol{e}$ is too close to both states **1** and **2** to allow this hypothesis. However, DMST uses this assumption anyway, as it is a method that seeks very fast convergence through simple modeling. State $\boldsymbol{e}$ acts as the output state for Disk 1 and as the input state for Disk 2.

4. State **2**: this is the state of the flow when interacting with the downwind actuator disk, also called the rear half-cycle of the turbine.

5. State $\boldsymbol{w}$: this is the wake state. The flow is perturbed by both Disks 1 and 2. It acts as the output state for Disk 2.

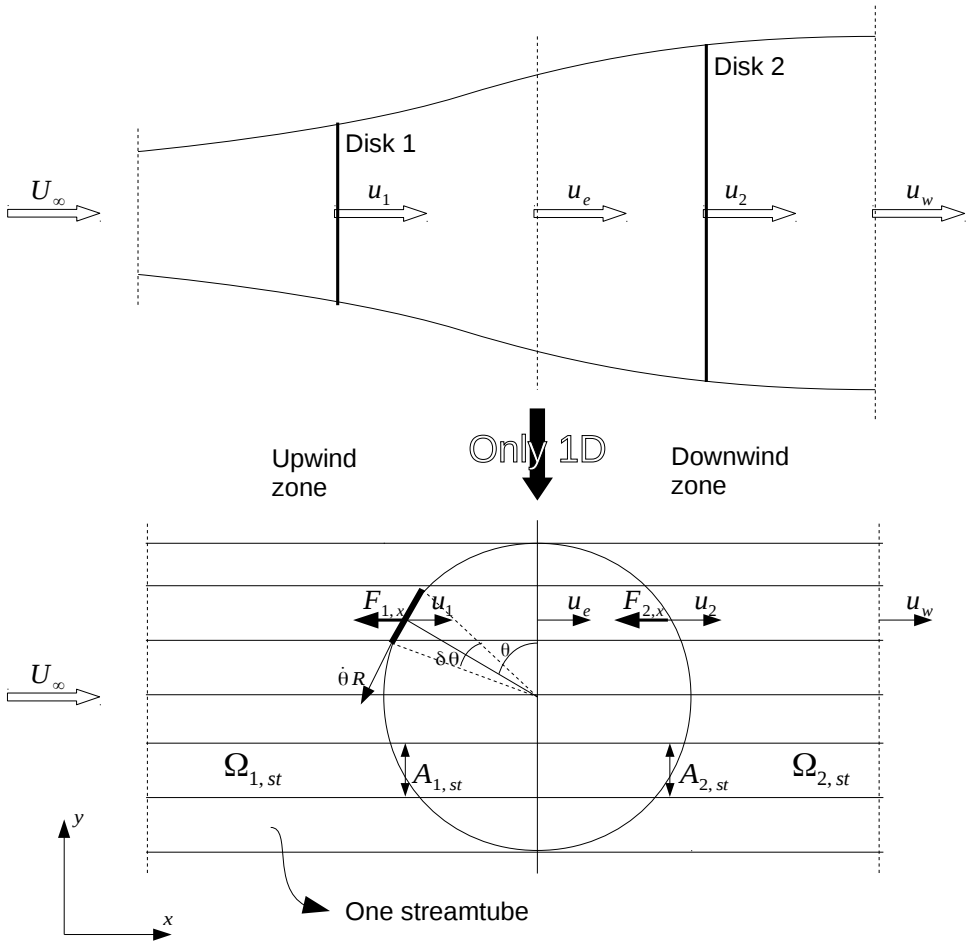

Figure 2.2: **Scheme of the DMST discretization of a VAWT domain.**

According to Figure 2.2, if one considers each streamtube of angular width $\delta\theta$ as being infinitesimally thin – which means that $\delta\theta \to 0$ – its swept area can be computed as

$$A_{1,st} = R\,\delta\theta\,\sin\theta_{st}\ , \qquad \forall\,\theta_{st} \in (0,\pi)\ , \tag{2.12a}$$

$$A_{2,st} = R\,\delta\theta\,(-\sin\theta_{st})\ , \qquad \forall\,\theta_{st} \in (\pi,2\pi)\ , \tag{2.12b}$$

where θ_{st} is the value of θ the blade has when it is going through the middle point of the given streamtube.

Now, conservation equations can be applied. Equation 2.1 mathematically ex-

presses the fact that there is no mass exchange between streamtubes: each streamtube mass flow ($\dot{m}_{st}$) is constant. Therefore, for each streamtube with section $A_{i,st}$:

$$\dot{m} = \rho\, u_1\, A_{1,st} = \rho\, u_2\, A_{2,st} = ct. \tag{2.13}$$

Equation 2.2, once evaluated in one front and one back streamtube in the direction parallel to the flow, gives the expressions[5]

$$\dot{m}\,(u_e - U_\infty) = -F_{1,x}\ , \tag{2.14a}$$

$$\dot{m}\,(u_w - u_e) = -F_{2,x}\ . \tag{2.14b}$$

Similarly, from Equation 2.3, one obtains

$$\frac{1}{2}\,\dot{m}\,(u_e^2 - U_\infty^2) = -F_{1,x}\,u_1\ , \tag{2.15a}$$

$$\frac{1}{2}\,\dot{m}\,(u_w^2 - u_e^2) = -F_{2,x}\,u_2\ . \tag{2.15b}$$

Using the interference factor: $\lambda_1 = u_1/U_\infty$ and $\lambda_2 = u_2/u_e$, and combining Equations 2.14 and 2.15, the velocities[6] of the equilibrium and wake states,

$$u_e = U_\infty\,(2\,\lambda_1 - 1)\ , \tag{2.16a}$$

$$u_w = u_e\,(2\,\lambda_2 - 1)\ , \tag{2.16b}$$

and that of the rear half-cycle,

$$\frac{u_2}{U_\infty} = (2\,\lambda_1 - 1)\,\lambda_2\ , \tag{2.17}$$

---

[5]Note that, from now on, the subscript $_{st}$ is omitted on all forces and velocities, as they all refer only to a single streamtube

[6]Note that flow velocity expressions violate continuity (Equation 2.13). In an incompressible flow, by considering that there is no streamtube expansion and no spanwise components of the velocity, flow velocity should be constant, as noted previously in this chapter.

are found.

Using the thrust coefficient expression – $C_{F_{1,x}} = F_{1,x}/(1/2\,\rho\,A_{1,st}\,U_\infty^2)$, for the front half-cycle, and $C_{F_{2,x}} = F_{2,x}/(1/2\,\rho\,A_{2,st}\,u_e^2)$, for the rear one – and combining Equations 2.13, 2.14 and 2.16, the thrust coefficient expression from the conservation analysis,

$$C_{F_{i,x}} = 4\,\lambda_i(1-\lambda_i)\ , \qquad \forall i = 1,2\ , \tag{2.18}$$

is obtained. However, due to the inadequacy of the unidirectional flow assumption below $\lambda \approx 0.6$, Glauert [5] proposed a linear modification to this result,

$$C_{F_{i,x}} = \begin{cases} 1849/900 - 26\,\lambda_i/15 & : \lambda_i < 43/60 \\ \\ 4\,\lambda_i(1-\lambda_i) & : \lambda_i \geq 43/60 \end{cases}\ , \qquad \forall i = 1,2\ , \tag{2.19}$$

according to experimental data.

To be able to solve the interference factor, another expression for the thrust at any given azimuthal angle,

$$F_{i,x}(\theta) = \frac{1}{2}\,\rho\,c\,u_{i,r}^2\,(C_D\,\cos\beta - C_L\,\sin\beta)\ , \qquad \forall i = 1,2\ , \tag{2.20}$$

is needed. This expression is obtained from load analysis. As shown in Equation 2.9, lift and drag coefficients can be used to obtain the instantaneous thrust each blade receives. Then, Equation 2.20 is time-averaged along one period in one single streamtube of width $\delta\theta$ for all the N_b blades of the turbine. This results in

$$F_{i,x} = \frac{N_b}{2\pi}\int_{\theta_{i,st}-\delta\theta/2}^{\theta_{i,st}+\delta\theta/2} F_{i,x}(\theta)\,\mathrm{d}\theta = \frac{N_b\,\delta\theta}{2\pi}\,F_{i,x}(\theta_{i,st})\ , \qquad \forall i = 1,2\ . \tag{2.21}$$

The reader will note that this integral is solved with a first order approximation. Then, using the thrust coefficient expressions, together with Equations 2.12, 2.20 and 2.21, the other expression for the thrust coefficient at each streamtube,

$$C_{F_{1,x}} = \frac{\sigma}{\pi\,\sin\theta}\,\frac{u_{1,r}^2}{U_\infty^2}\,(C_D\,\cos\beta - C_L\,\sin\beta)\ , \qquad \forall i = 1,2\ , \tag{2.22a}$$

$$C_{F_{2,x}} = \frac{-\sigma}{\pi\,\sin\theta}\,\frac{u_{2,r}^2}{U_\infty^2\,(2\,\lambda_1 - 1)}\,(C_D\,\cos\beta - C_L\,\sin\beta)\ , \qquad \forall i = 1,2\ , \tag{2.22b}$$

are obtained.

By using Equations 2.19 and 2.22, $\lambda_1(\theta)$ and $\lambda_2(\theta)$ can both be computed – note that λ_1[7] participates in Equation 2.22b, so the flow going through the front half-cycle must be solved before it can be solved in the rear half-cycle, too. Also see that this system can be solved for any value of θ – that is why the interference factors are using dependence notation (θ). Remember that $\delta\theta \to 0$, so there are an infinite number of streamtubes. Then, the first order approximation introduced in the integral of Equation 2.21 does not limit the order of precision of the whole problem. Instead, it will be limited by the algorithms used to solve this system and to integrate the torque along the blade path, needed to average the output power of the turbine.

From the interference factor, all variables ($\beta(\theta)$, $\alpha(\theta)$, velocities, force coefficients, etc.) can be obtained using the equations shown in Section 2.2.2. Then, each blade non-dimensional torque at any given azimuthal angle is

$$C_{T_b}(\theta) = \frac{T_b(\theta)}{1/2\,\rho\,c\,U_\infty^2\,R} = \frac{u_r^2}{U_\infty^2}\,(C_L\,\boldsymbol{l} + C_D\,\boldsymbol{d})\cdot\boldsymbol{\tau}\ , \tag{2.23}$$

according to Equation 2.10.

To obtain the whole instantaneous torque coefficient using turbine parameters, $C_T(\theta) = T(\theta)/\left(1/2\,\rho\,A\,U_\infty^2\,R\right)$, one should add the instantaneous torque of each blade. Note that the swept area is $A = 2R$ because this is a 2D case. Then a turbine with N_b equidistant blades, b_i, $\forall i \in [1, N_b]$, would be subject to the total torque coefficient,

$$C_T(\theta) = \frac{\sigma}{N_b}\sum_{i=1}^{N_b} C_{T_{b_i}}\left(\theta + \frac{i-1}{3}\,2\pi\right)\ . \tag{2.24}$$

Note that for any N_b number of blades, distributed equidistantly, the whole torque coefficient has a periodicity of $2\pi/N_b$. Also, please notice that θ is the azimuthal angle of the first blade, b_1.

---

[7]For $\theta > \pi$, note that the value of λ_1 inserted in Equation 2.22b is $\lambda_1(2\pi - \theta)$

Finally, the power coefficient that all blades produce, $C_P = P/(1/2\,\rho\,A\,U_\infty^3)$, is

$$C_P = C_{P,1} + C_{P,2} \ , \tag{2.25}$$

where $C_{P,1}$ and $C_{P,1}$,

$$C_{P,1} \equiv C_{P,\text{front}} = \frac{\sigma\,TSR}{2\pi} \int_0^\pi C_{T_b}\,\mathrm{d}\theta \ , \tag{2.26a}$$

$$C_{P,2} \equiv C_{P,\text{back}} = \frac{\sigma\,TSR}{2\pi} \int_\pi^{2\pi} C_{T_b}\,\mathrm{d}\theta \ , \tag{2.26b}$$

are obtained by averaging the instantaneous power in each half-cycle, according to Equation 2.11.

This method, although requiring some numerical calculations to solve the interference factor equation and to numerically integrate the torque to obtain the power, is very straightforward and easy to implement. However, it neglects several effects that gain great relevance in the case of wind turbines. The most significant are the effect of the blades working in angles of attack beyond the static stall angle, the unsteadiness nature of the problem (which includes the effects of dynamic stall) and the interaction of the blades and the wakes that detach from themselves. Also, the 1D simplification introduces some error by neglecting span-wise velocity and 3D effects on the blade.

2.3 Computational algorithm

No analytical solution of $\lambda(\theta)$ exists, so no analytical integration of the torque – in order to get the power – can be computed either. Therefore, numerical integration is necessary to obtain the performance characteristics of the VAWT. Also, as the resulting equation from combining Equations 2.19 and 2.22 is nonlinear, another numerical procedure is required to solve it.

The results described in this report have been obtained by using a second-order

CHAPTER 3

DYNAMIC STALL MODELS

3.1 Concepts

As mentioned in the previous chapter, dynamic stall plays a very relevant role in the VAWT problem. However, static lift and drag curves have been used. Obviously there is significant amount of error introduced by this fact. Therefore, a lot of effort has been invested into developing modifications to the original DMST, so that it includes these effects. Dynamic stall, opposite to the usual static stall observed in wind tunnels – and in fixed blades simulations –, presents a hysteresis behavior. In other words, if a blade changes its position, the flow does not react immediately, but it adapts gradually to the new state within a definite interval of time. Such an effect is only dominant at low TSR, when the turbine rotates slowly enough to allow the development of this hysteresis cycle – the magnitude of the blade movement is similar or smaller than that of the flow movement. In high TSR cases this effect ceases to be determinant – wake interactions gain strength and become the major factor. In this latter case, the induced velocity, $\dot{\theta}\,R$, component of the relative velocity, u_r, is much higher than the wind velocity component, U_∞ – see Figure 2.1. Therefore, angles of attack are lower, according to Equation 2.6, which leads to smaller oscillations of the blade respectively to the relative movement of the flow.

Most of the dynamic stall models, according to [18], applied to DMST consist of a series of semi-empirical procedures applied in the calculation of the lift and drag coefficients of the VAWT blade. Therefore, applying a dynamic stall model to the DMST method means computing some additional steps interlaced with the main algorithm.

3.2 Theory development

In this section, several dynamic stall models are explained and compared. These are:

3.2.1 Gormont model

Gormont [6] proposed this method to take into account dynamic stall in helicopter blades. It is not optimal for VAWTs, because they operate at much higher angles of attack, but it has been used as a very strong base for later adaptations. The Gormont method consists of applying a certain delay,$\delta\alpha$, on the angle of attack, based on hysteresis behavior. After applying this delay, the resulting reference angle of attack is

$$\alpha_{ref} = \alpha - K\,\delta\alpha\ , \tag{3.1}$$

where K,

$$K = \begin{cases} 1 & : \dot{\alpha} \geq 0 \\ & \\ -0.5 & : \dot{\alpha} < 0 \end{cases}\ , \tag{3.2}$$

is a parameter defined according to Gormont's empirical observations.

Therefore, the delay experienced when the absolute angle of attack is increasing is twice the one observed when it is decreasing. One possible qualitative explanation would be the following. When the angle of attack is increasing, the flow near the leading edge of the blade is *pushed* to the surface of it, making it more difficult for the upwind flow to change its state. However, when the blade angle of attack is decreasing, this same flow is *left behind*, so the upwind flow changes its state more easily. This effect generates a discontinuity that can induce severe instabilities to the flow surrounding the points where $\dot{\alpha}$ changes sign[9].

[9] $\dot{\alpha}$ is the rate of change of the absolute value of α, so it is negative when the angle of attack approaches 0 and positive when it moves away from 0.

The term $\delta\alpha$ is proportional to the non-dimensional rate parameter S,

$$S = \sqrt{\left|\frac{c\,\dot{\alpha}}{2u_r}\right|}\ , \tag{3.3}$$

which can also be interpreted as the square root of the magnitude of the leading edge velocity of a blade rotating around its half chord point over the magnitude of the relative wind velocity. In other words, it compares the blade movement to the flow relative movement around it. The higher S is, the greater the applied delay. This is coherent with what was explained in Section 3.1 – dynamic stall is important for low tip-speed ratios, when α oscillations are bigger.

The slope of the line $\delta\alpha(S)$ decreases both with thickness over chord ratio and Mach number of the flow relative to the blade growth. Then, the thicker the blade is and the less compressible the flow is, the smaller is the delay on the angle of attack. The specific expression for $\delta\alpha$ can be found Appendix C.

Once the delayed angle of attack, α_{ref}, is found, the modified lift and drag coefficients can be calculated. The lift coefficient,

$$C_L^{dyn} = C_{L,0}(\alpha_0) + m\,(\alpha - \alpha_0)\ , \tag{3.4}$$

is calculated by using the potential equation with a modified slope, m, the minimum value of either the slope of the linear part of C_L or the value obtained with the following expression: $(C_L(\alpha_{ref}) - C_L(\alpha_0))/(\alpha_{ref} - \alpha_0)$. Figure 3.1 shows both mentioned slopes for an example value of α_{ref}. Also, the mathematical expression for m can be found in Appendix C. The symbol α_0 refers to the angle of attack at zero lift.

The drag coefficient,

$$C_D^{dyn} = C_D(\alpha_{ref})\ , \tag{3.5}$$

is obtained simply by using α_{ref} to extract it from the available static data.

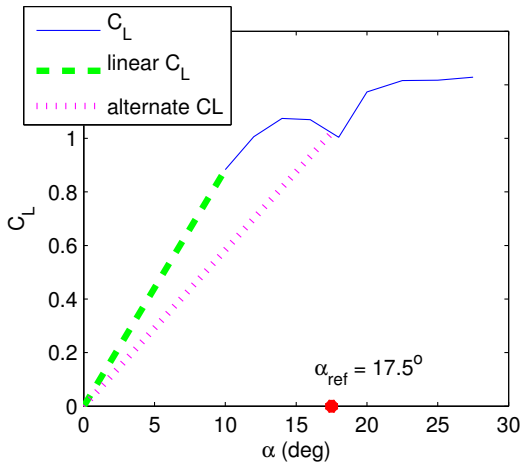

Figure 3.1: **The two different values from which the C_L^{dyn} slope is calculated.** In this example, the value used would be the slope of the dotted line, because it is lower.

3.2.2 Berg modification

Berg [3] considered that the α range at which helicopter blades work is much lower than that of a VAWT, which can perfectly go beyond the stall angle of attack (α_{ss}). Therefore, Berg theorized that the pure Gormont method might over predict the lift and drag for high angles of attack. He proposed the following modification for both lift,

$$C_L^{mod} = \begin{cases} C_L + \left[\frac{A_M\,\alpha_{ss}-\alpha}{A_M\,\alpha_{ss}-\alpha_{ss}}\right]\,(C_L^{dyn} - C_L) & : \alpha \leq A_M\,\alpha_{ss} \\ C_L & : \alpha > A_M\,\alpha_{ss} \end{cases}, \tag{3.6}$$

and drag[10], so that both coefficients tend to the static values for very high values of α, deep into the non-linear regime. The parameter A_M is set by the user of the method. According to [3] the best option is $A_M = 6$. However, according to [18], some VAWTs show a better response when using $A_M \to \infty$. Note that this is the

[10]Only the lift modification is shown. The drag modification is the same expression but changing all $_L$ subscripts for $_D$. See Appendix C for the drag expression.

same as using the pure Gormont method with no modifications. The results shown on this paper are computed using Berg's suggestion.

3.2.3 Strickland *et al.* adaptation

Strickland *et al.* [25] considered that Gormont method was developed for very thin blades, as the typical helicopter blade. However, VAWTs typically use blades with higher thickness over chord ratio. That is why they modified the delay so $S_c = 0$. See Equation C.2 in Appendix C. Also, as the typical rotation speed of a VAWT is much lower than that of a helicopter, the flow was considered to be incompressible – the Mach number is not used as an input parameter of the model. Finally, Strickland *et al.* supposed that dynamic stall effects only occur after the angle of attack is higher than the stall angle of attack, $\alpha \geq \alpha_{ss}$. Then, the resulting reference angle of attack is:

$$\alpha_{ref} = \alpha - \gamma\, K\, S\, S_{\dot{\alpha}}\ , \tag{3.7}$$

where K and S are described in Equations 3.2 and 3.3, respectively. $S_{\dot{\alpha}}$ is the sign of $\dot{\alpha}$ as is described in Section 3.2.1. Expression for γ can be found in Appendix C.

From Strickland's angle of attack, lift,

$$C_L^{str} = \begin{cases} C_L(\alpha) & : \alpha < \alpha_{ss} \\ \left(\frac{\alpha}{\alpha_{ref} - \alpha_0}\right) C_L(\alpha_{ref}) & : \alpha \geq \alpha_{ss} \end{cases}\ , \tag{3.8}$$

and drag,

$$C_D^{str} = \begin{cases} C_D(\alpha) & : \alpha < \alpha_{ss} \\ C_D(\alpha_{ref}) & : \alpha \geq \alpha_{ss} \end{cases}\ , \tag{3.9}$$

coefficients are obtained.

3.2.4 Paraschivoiu adaptation

Paraschivoiu [17], after some experimental observation, concluded that the

part of the blade path comprised in $\theta \in [105°, 225°]$ is mainly dominated by turbulent aerodynamics and wake interactions. Therefore, they considered that in this region dynamic stall can be neglected. Therefore, their modification basically consists of applying Strickland adaptation only outside this azimuthal angle range. This adaptation might be a bit crude, because it is based on experimental data from one specific turbine under some very particular conditions.

3.2.5 Indicial method and adaptations

Another different approach to dynamic stall modeling is the indicial method. It was first introduced by Beddoes and Leishman [2] and first applied to VAWTs by Paraschivoiu *et al.* [19]. This method consists of accepting that the total effect of lift and drag modification due to dynamic stall results of the individual addition of different effects. The first step consists on calculating the attached flow unsteady behavior by using potential flow theory and the addition of unsteady empirical correlations. Second, separation in the leading and trailing edge are taken into account. Finally, an optional third phase introduces some corrections of the separation for deep stall, when the angle of attack is far beyond the stall angle of attack. All these effects are supposed to have indicial behavior. This means that they grow or decrease with time according to lag and impulsive functions. These indicial functions are of the form of summations of exponential functions with different coefficients and characteristic time parameters. All modifications depend also on the rate of change over time of the angle of attack, as did the Gormont based models.

This method, however, depends on several coefficients – mainly the lag and impulsive parameters – that must be determined empirically and/or by potential flow approximations. Also, it considerably increases the computational requirements, because the introduced modifications must be solved by iterative methods, which DMST must apply at every iteration of the interference factor calculation. According

to [18], the indicial method gives an overall better approximation of the dynamic stall models than the Gormont based ones. However, for qualitative purposes the difference is not very high compared to Berg adaptation, for example. For all these reasons, the indicial method is not explained nor was developed during the redaction of this report. More information can be found in [18]. Further development on streamtube models must include the development of DMST code with Indicial dynamic model.

Several adaptations of the original Beddoes and Leishman model have been applied to wind turbines in general, such as Hansen [7].

3.3 Computational algorithm modifications

In order to insert any of the described dynamic stall models into the DMST algorithm proposed in Section 2.3, three additional steps must be introduced. Basically, *Compute* C_L, C_D box of each Figure 2.3, 2.4 and 2.5 must be substituted by the specific calculation of the modified lift and drag coefficients. The flowchart for the modified DMST of the front half is shown in Figure 3.2. The rest of the algorithm can be found in Appendix C.

CHAPTER 4

WAKE INTERACTION

4.1 Concepts

Wake interaction is the effect of the turbulent wakes generated by the blades on the front half received on the back half. However, BEMT is unable to model turbulence, so wake interaction is neglected in streamtube models. Also, modeling this effect by using the fundamental physics that describe turbulence – or some turbulence model – and applying it directly to streamtube models would be very detrimental to the computational efficiency of BEMT – in fact, the problem would become a mixture of BEMT and a grid-centered algorithm. BEMT's main advantage, actually, is computational efficiency. Therefore, a workaround was needed. Kozak [9] studied the turbine described on Table 2.1 with a grid-centered method. He used STAR-CCM+ [23] to apply 2D finite volume discretization to the Navier–Stokes equations. Kozak and Vallverdú *et al.* [10] compared the effective angle of attack obtained from Vallverdú's code [30] with dynamic stall – the green curve in Figure 3.8 – with Kozak's own results shown on [9]. From this comparison, they were able to develop a much simpler and effective wake interaction model for DMST that was shown to correlate well with finite volume simulation.

4.2 Theory development

The Kozak *et al.* wake model follows the subsequent observation. By studying graphic visualizations of the vorticity generated by the blades [9] – see Figure 4.1 –, they realized that the number of wakes,

$$N_w = 0.85\, N_b\, TSR\ , \tag{4.1}$$

that exist in the rear half of the turbine at a given moment is proportional to the tip speed ratio and the number of blades.

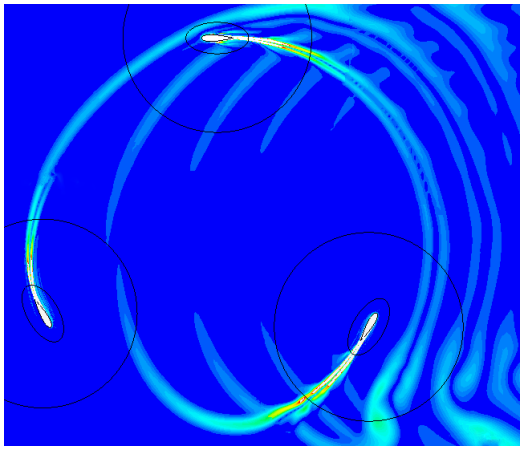

Figure 4.1: **Visualization of the vorticity for $TSR = 3$ [9].**

Also, they observed that each blade hits each wake twice. They considered that the width of a wake is equal to the thickness of a blade. This hypothesis neglects the wake diffusion, but it is accurate enough for streamtube application. Therefore, a distance value,

$$d_w = 2\, t\, N_w\ , \tag{4.2}$$

can be obtained. This distance, d_w, represents the sum of all the parts of the blade path that crosses a wake. However, this value is more useful if used as a ratio,

$$r_w = \frac{d_w}{\pi\ R}\ , \tag{4.3}$$

where the denominator is the distance covered by a blade in the rear half-cycle of the turbine. Note that r_w does not depend anymore on the number of blades of the turbine, because both numerator and denominator include the number of blades, hence it disappears. It represents the proportion of the blade path in the back that cuts through a wake.

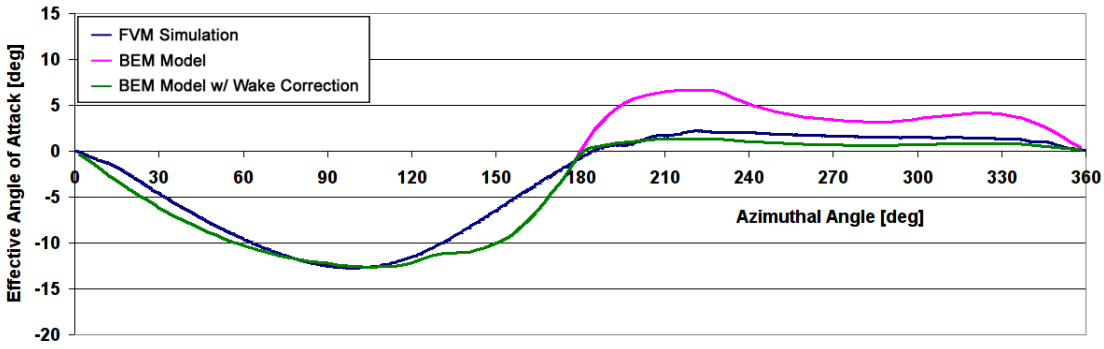

Figure 4.2: **Effective angle of attack comparison between Kozak and Vallverdú results for $TSR = 3$ [10].**

Kozak and Vallverdú *et al.* assumed that the flow inside the wake travels at the same speed and with the same direction than the blade that generated it. Therefore, according to that assumption, when a blade hits a wake in the rear part, its relative velocity is diminished a lot, and so does its instantaneous angle of attack. In other words, when a blade hits a wake, its lift and drag coefficients decrease dramatically. This hypothesis may seem to be very crude, because it neglects several diffusion and transport effects. Also, the blade and the wake do not hit in parallel directions. However, following this line of thought, Kozak and Vallverdú *et al.* multiplied Vallverdú's results of the rear half-cycle effective angle of attack by the $(1 - r_w)$ term – they dropped lift and drag down to zero whenever a blade hits a wake. Afterwards, they compared the output with Kozak's [9] effective angle of attack: the result was very satisfactory. Both curves, in the range of $\theta \in [\pi, 2\pi]$ fit almost perfectly – see

Figure 4.2 for the $TSR = 3$ example[13]. Hence, the hypothesis taken related to the flow motion in the wake proves not to be so wrong.

The effective angle of attack, as said before, is basically a representation of the lift coefficient. Therefore, both Kozak and Vallverdú *et al.* [10] concluded that the wake effect could be included in a simple way in streamtube model by reducing both final lift and drag coefficients by r_w,

$$C_L^{wake} = \begin{cases} C_L^{dyn} & : \theta \in (0, \pi) \\ C_L^{dyn}(1 - r_w) & : \theta \in (\pi, 2\pi) \end{cases}, \tag{4.4a}$$

$$C_D^{wake} = \begin{cases} C_L^{dyn} & : \theta \in (0, \pi) \\ C_L^{dyn}(1 - r_w) & : \theta \in (\pi, 2\pi) \end{cases}. \tag{4.4b}$$

This reduction should be applied after the determination of the interference factor but before the postprocessing – in other words, before the calculation of torque and power coefficient.

Note that the wake interaction is approached as an average effect on the whole rear half-cycle of the turbine. However, the real wake interaction is a very discrete effect [9].

[13]Curves for other values of TSR can be found in [10].

BIBLIOGRAPHY

[1] Wind Energy Foundation. `http://www.windenergyfoundation.org/about-wind-energy/history`. Accessed on June 15th 2014.

[2] T. S. Beddoes and J. G. Leishman. A SemiEmpirical Model for Dynamic Stall. *Journal of the American Helicopter Society*, 34(3):3–17, July 1989.

[3] D. E. Berg. Improved Double-Multiple Streamtube Model for the Darrieus-type Vertical Sxis Wind Turbine. *Presented at the Am. Solar Energy Soc. Meeting, Minneapolis*, 1983.

[4] A. Betz. Das Maximum der theoretisch möglichen Ausnutzung des Windes durch Windmotoren. *Zeitschrift für das gesamte Turbinenwesen*, 26:307–309, 1920.

[5] H. Glauert. Airplane Propellers. In *Aerodynamic Theory*, pages 169–360. Springer Berlin Heidelberg, 1935.

[6] R. E. Gormont and Boeing Vertol Company. A Mathematical Model of Unsteady Aerodynamics and Radial Flow for Application to Helicopter Rotors. Technical Report AD-767 240, Army Air Mobility Research and Development Laboratory, Philadelphia, Pa, May 1973. Distributed by National Techinical Information Service.

[7] M. H. Hansen, M. Gaunaa, and H. A. Madsen. A Beddoes-Leishman type dynamic stall model in state-space and indicial formulations. Technical Report Risøo-R-1354(EN), Risøo National Laboratory, Roskilde, Denmark, June 2004.

[8] P. Holtberg et al. International Energy Outlook 2013. Technical Report DOE/EIA-0848(2013), U.S. Energy Information Administration, Washington, DC, July 2013. `http://www.eia.gov/forecasts/ieo/world.cfm`.

[9] P. A. Kozak. Effects of Unsteady Aerodynamics on Vertical-Axis Wind Turbine Performance, 2014.

[10] P. A. Kozak, D. Vallverdú, and D. Rempfer. Modeling Vertical-Axis Wind Turbine Performance: Blade Element Method vs. Finite Volume Approach. To be submitted in the In Proceedings of The AIAA Propulsion and Energy Forum and Exposition 2014, 2014.

[11] H. C. Larsen. Summary of a Vortex Theory for Cyclogyro. In *Second US National Conference on Wind Engineering Research*, volume 8, pages 1–3. Colorado State University, 1975.

[12] D.G.J. Marie. Turbine having its rotating shaft transverse to the flow of the current, December 8 1931. US Patent 1,835,018.

[13] MATHEMATICA. *Version 9.0.1.* Wolfram Research, Champaign, Illinois USA, 2013.

[14] MATLAB. *Version 8.2.0.701 (R2013b).* The MathWorks Inc., Natick, Massachusetts USA, 2013.

[15] I. Paraschivoiu. Double-Multiple Streamtube Model for Darrieus Wind Turbines. *Second DOE/NASA Wind Turbines Dynamics Workshop*, pages 19–25, 1981. NASA CP-2185.

[16] I. Paraschivoiu. Aerodynamic Loads and Performance of the Darrieus Rotor. *AIAA Journal of Energy*, 6:406–412, November 1982.

[17] I. Paraschivoiu. Double-Multiple Streamtube Model for Studying Vertical-Axis Wind Turbines. *AIAA Journal of Propulsion and Power*, 4:370–378, 1988.

[18] I. Paraschivoiu. *Wind Turbine Design With Emphasis on Darrieus Concept*. Number ISBN 2-553-00931-3. Polytechnic International Press, Montréal, Canada, 2002. École Polytechnique de Montréal.

[19] I. Paraschivoiu and S. R. Major. Indicial Method calculating Dynamic Stall on a Vertical-Axis Wind Turbine. *Journal of Propulsion and Power*, 8(4):909–911, 1992.

[20] S.J. Savonius. Wind rotor, June 1930. US Patent 1,766,765.

[21] Daniel. Shepherd, David. McBride, David. Welch, Kim. Dirks, and Erin. Hill. Evaluating the impact of wind turbine noise on health-related quality of life. *Noise and Health*, 13(54):333–339, 2011.

[22] P.R. Spalart and Allmaras. A one-equation turbulence model for aerodynamic flows. In *30th Aerospace Sciences Meeting and Exhibit*, January 1992.

[23] STAR-CCM+. *Version 9.02.007 (9)*. CD-adapco, Melville, New York USA, 2014.

[24] J.H. Strickland and Sandia Laboratories. Advanced Energy Projects Dept. *The Darrieus Turbine: A Performance Prediction Model Using Multiple Streamtubes*. SAND. Sandia Laboratories, 1975.

[25] J.H. Strickland, T. Nguyen, B.T. Webster, Sandia National Laboratories, and United States. Department of Energy. *A Vortex Model of the Darrieus Turbine: An Analytical and Experimental Study*. Sandia Laboratories, 1980.

[26] G. V. Subashki and D. Rempfer. Mathematica streamtube VAWT code. Personal contact.

[27] H. J. Sutherland, D. E. Berg, and Ashwill T. D. A Retrospective of VAWT Technology. Technical Report SAND2012-0304, Sandia National LAboratories, Albuquerque, NM and Livermore, CA, January 2012.

[28] R. J Templin and National Aeronautical Establishment (Canada). Aerodynamic Performance Theory for the NRC Vertical-Axis Wind Turbine. 1974. Reproduced by National Technical Information Service.

[29] Boston University. Wind Turbines. `http://people.bu.edu/noahb/files/wind_turbine_main.pdf`. Accessed on June 17$^{\text{th}}$ 2014.

[30] D. Vallverdú, D. Rempfer, and P. A. Kozak. VAWT Analysis. `http://www.mathworks.com/matlabcentral/fileexchange/46909-vawt-analysis`, June 2014. Published in Mathworks File Exchange.

APPENDIX C

DYNAMIC STALL NEEDED EXPRESSIONS

This Appendix contains the needed expressions for the stall models that are note physically interpretable and hence not suitable for the main report.

C.1 Gormont method

$$\delta\alpha = \begin{cases} \gamma_1 \, S & : S \leq S_c \\ \gamma_1 \, S_c + \gamma_2 \, (S - S_c) & : S > S_c \end{cases} \tag{C.1}$$

$$S_c = 0.006 + 1.5 \left(0.006 - \frac{t_c}{c} \right) \tag{C.2}$$

$$\gamma_1 = \begin{cases} \frac{\gamma_2}{2} & : \text{for lift characteristic} \\ 0 & : \text{for drag characteristic} \end{cases} \tag{C.3}$$

$$\gamma_2 = \gamma_{max} \, \max \left\{ 0, \min \left[1, \frac{M - M_2}{M_1 - M_2} \right] \right\} \tag{C.4}$$

$$\gamma_{max} = \begin{cases} 1.4 + 6.0 \, (0.06 - \frac{t_c}{c}) & : \text{for lift characteristic} \\ 1.0 + 2.5 \, (0.06 - \frac{t_c}{c}) & : \text{for drag characteristic} \end{cases} \tag{C.5}$$

$$M_1 = \begin{cases} 0.4 + 5.0 \, (0.06 - \frac{t_c}{c}) & : \text{for lift characteristic} \\ 0.2 & : \text{for drag characteristic} \end{cases} \tag{C.6}$$

$$M_2 = \begin{cases} 0.9 + 2.5 \, (0.06 - \frac{t_c}{c}) & : \text{for lift characteristic} \\ 0.7 + 2.5 \, (0.06 - \frac{t_c}{c}) & : \text{for drag characteristic} \end{cases} \tag{C.7}$$

$$m = \min\left[\frac{C_L(\alpha_{ref}) - C_L(\alpha_0)}{\alpha_{ref} - \alpha_0}, \frac{C_L(\alpha_{ss}) - C_L(\alpha_0)}{\alpha_{ss} - \alpha_0}\right] \tag{C.8}$$

C.2 Berg modification

$$C_D^{mod} = \begin{cases} C_D + \left[\frac{A_M\,\alpha_{ss} - \alpha}{A_M\,\alpha_{ss} - \alpha_{ss}}\right]\,(C_D^{dyn} - C_D) & : \alpha \leq A_M\,\alpha_{ss} \\ C_D & : \alpha > A_M\,\alpha_{ss} \end{cases} \tag{C.9}$$

C.3 Strickland adaptation

$$\gamma = \begin{cases} 1.4 - 6.0\,(0.06 - \frac{t_c}{c}) & : \text{for lift characteristic} \\ 1.0 - 2.5\,(0.06 - \frac{t_c}{c}) & : \text{for drag characteristic} \end{cases} \tag{C.10}$$

C.4 Computational algorithm modifications

See Figures C.1 and C.2.

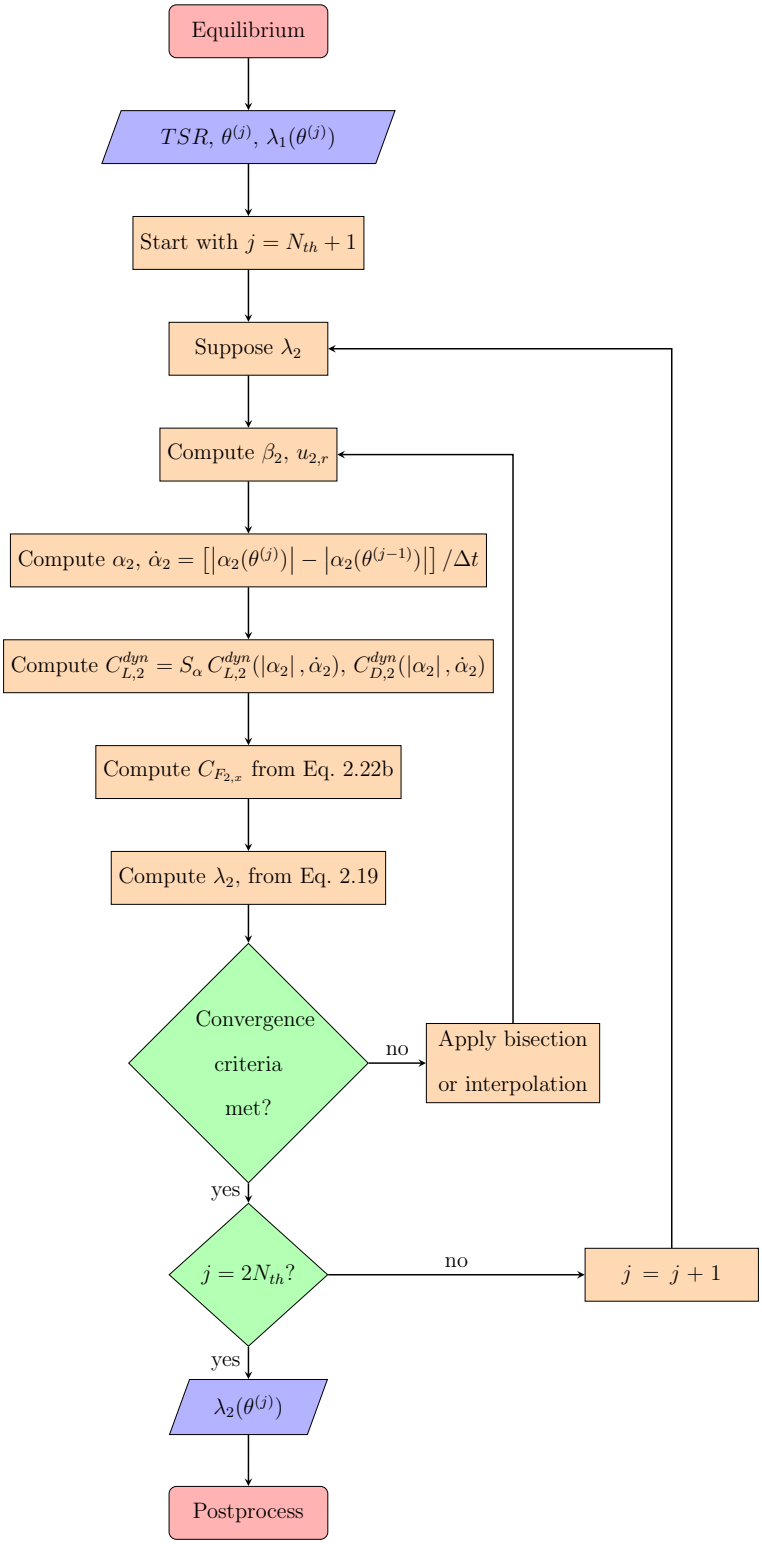

Figure C.1: **Flowchart of the calculation of $\lambda_1(\theta^{(j)})$ for the dynamic stall modification.**

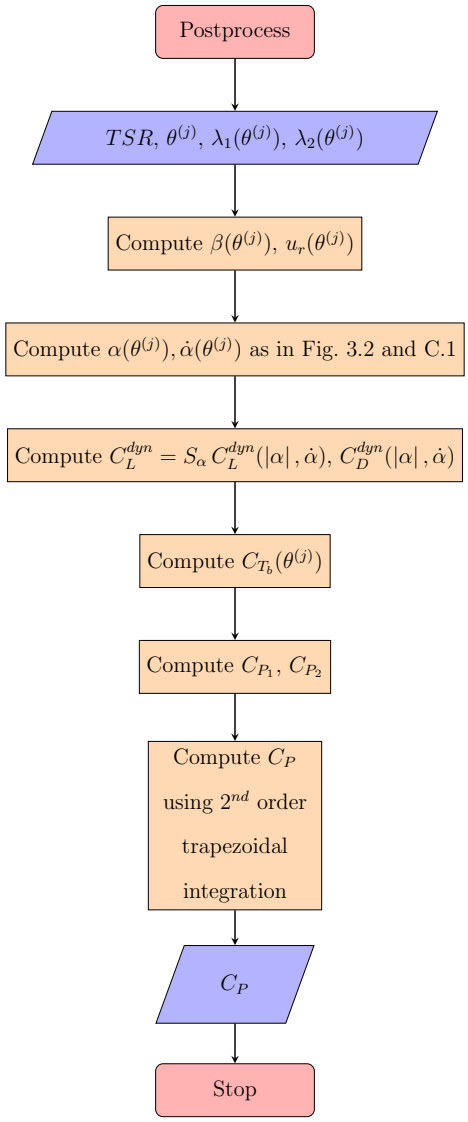

Figure C.2: **Flowchart of the calculation of C_P for the dynamic stall modification.**